

Atomic fountain clocks

R Wynands and S Weyers

Physikalisch-Technische Bundesanstalt, Bundesallee 100, 38116 Braunschweig, Germany

Received 26 April 2005

Published 7 June 2005

Online at stacks.iop.org/Met/42/S64

Abstract

We describe and review the current state of the art in atomic fountain clocks. These clocks provide the best realization of the SI second possible today, with relative uncertainties of a few parts in 10^{16} .

1. Introduction

One of the main objectives in decades of perfecting the caesium atomic clock has been the quest for ever increasing interaction times of the atoms with the microwave radiation [1]. Impressive results have been obtained by use of a combination of widely separated Ramsey zones and the magnetic selection of slow atoms [2]. However, intra-beam collisions and the velocity distribution in a thermal atomic beam make it difficult to select atoms much slower than 70 m s^{-1} , while geometric restrictions and the increasing influence of the exact shape of the velocity distribution on potential systematic frequency shifts place an upper limit on the useful Ramsey zone separation. For typical atom velocities of 100 m s^{-1} and a zone separation of 1 m one obtains an interaction time of 10 ms or a resonance linewidth of 50 Hz. This line has to be resolved with a signal-to-noise ratio (S/N) of the order of 10^6 to obtain the uncertainties of today's optically-pumped thermal beam clocks [3–5].

The advent of laser cooling techniques [6] opened the door to a radically new approach to the interaction time problem. Using a suitable arrangement of laser beams and magnetic fields one can capture caesium atoms from a thermal vapour and at the same time cool them down to just a few microkelvin above absolute zero temperature (figure 1(a)). Typically, in a few tenths of a second one can trap 10 million caesium atoms in a cloud a few millimetres in diameter and at a temperature of $2 \mu\text{K}$. At this temperature, the average thermal velocity of the caesium atoms is of the order of 1 cm s^{-1} , so the cloud of atoms stays together for a relatively long time. This cloud can be launched against gravity using laser light (figure 1(b)). Typically, the launch velocity is chosen such that the atoms reach a height of about one metre before they turn back and fall down the same path they came up. The motion of the cloud resembles that of the water in a pulsed fountain, hence the name 'fountain clock'.

On the way up and down the atoms pass through the same microwave cavity (figure 1(c)). The microwave power is chosen such that on each pass a $\pi/2$ pulse is experienced

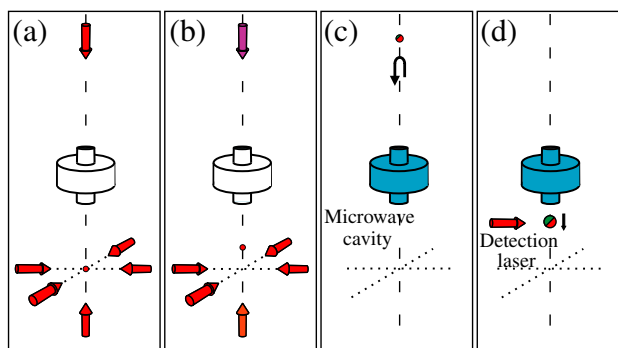


Figure 1. Principle of operation of the atomic fountain clock. (a) A cloud of cold atoms is trapped in the intersection region of six laser beams. (b) The cloud is launched by frequency detuning of the vertical lasers. (c) The cloud slowly expands during its ballistic flight in the dark. On the way up and on the way down it passes through a microwave cavity. (d) Detection lasers are switched on; they probe the population distribution by laser-induced fluorescence. (This figure is in colour only in the electronic version)

by the atoms. The two spatially separated Ramsey interactions of the thermal beam clock are thus replaced by two interactions in the same position but with reversed direction of travel. After the second interaction the state of the atom can be probed with the help of laser light (figure 1(d)). For a typical launch height of around half a metre above the microwave interaction zone it is possible to achieve effective interaction times of more than half a second. The resulting hundred-fold reduction in microwave resonance linewidth (figure 2) is the most obvious advantage of the fountain clock over the thermal beam clock.

Equally important is the reduction in the influence of certain systematic effects because the atoms are so slow. Furthermore, the trajectory reversal eliminates the end-to-end cavity phase shift and greatly reduces the influence of distributed cavity phases caused by an imperfect microwave field inside the cavity.

We will now give a short historical overview of the development of atomic fountain clocks before treating in greater detail the operation of a typical fountain clock,

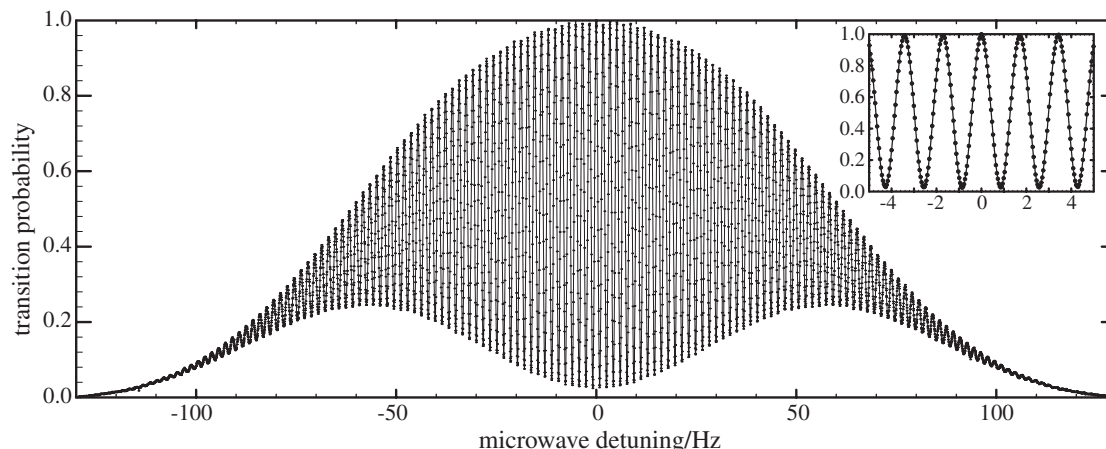


Figure 2. Measured Ramsey fringe pattern for PTB's CSF1 fountain clock (dots). Inset: the central part enlarged. The solid lines are there to guide the eye.

the sources of uncertainty and recent improvements and trends.

2. A brief history of fountain clocks

The first experiments exploring the fountain principle were performed by Zacharias [7] in the 1950s, using a thermal atomic beam directed upwards. Unfortunately, the desired selection of the very slowest atoms from the thermal distribution did not work because collisions near the nozzle of the oven practically eliminated this velocity class. A refined proposal was made in 1982 by De Marchi [8], for a thermal beam source. He predicted that with an optical selection of slow atoms and a special microwave cavity geometry 10^{-15} relative uncertainty could be reached for such a thermal fountain 3 m in height.

The main problem for fountains using thermal beams is that there are just not enough slow atoms in the thermal beam to give a sufficiently strong signal. The situation changed completely when laser cooling techniques allowed one to prepare cold atom samples containing millions of atoms, and all of them with basically the same velocity. The potential of such laser-cooled samples in a fountain geometry was considered by Hall *et al* [9] both for microwave and optical transitions and simultaneously realized by Kasevich *et al* [10]. In the latter experiment, a laser-cooled sodium cloud was launched by a laser pulse and entered a radio-frequency waveguide where it reached its apogee. While in the waveguide the atoms were illuminated with two $\pi/2$ pulses and then fell down through an ionization detection zone. A width of the central Ramsey fringe of 2 Hz was obtained in this way.

The first fountain for metrological use was developed at the Observatoire de Paris/France [11]. Its design [12] became a standard for almost all subsequently constructed fountain clocks, except for variations in the relative spatial arrangement of the cavities and the detection zone. In the late 1990s the fountains NIST-F1 at the National Institute of Standards and Technology (NIST) in Boulder/USA [13] and CSF1 at Physikalisch-Technische Bundesanstalt (PTB) in Braunschweig/Germany [14] became operational as primary standards. Recently, they were joined by the caesium fountain

clocks CsF1 at the Istituto Elettrotecnico Nazionale (IEN) in Torino/Italy [15] and CsF1 at the National Physical Laboratory (NPL) in Teddington/UK [16]. With FO2 and FOM [17] the Observatoire de Paris (Systèmes de Référence Temps-Espace—SYRTE) is operating two more primary fountain clocks. A number of other laboratories are currently operating or developing fountain clocks (see [18–27] for an incomplete list of examples). Most of these employ caesium as the active element.

In the following we will concentrate mostly on the seven primary caesium fountain clocks in operation today since they have been the most thoroughly characterized ones and more information is available on them.

3. Operation of a fountain clock

Figure 3 shows a simplified set-up of the vacuum subsystem of a fountain clock. Six laser beams cross in the centre of the preparation zone, where the cold atomic cloud is produced (section 3.1). Above that follows the detection zone which is traversed by laser beams for fluorescence detection of the falling cloud (section 3.3). The microwave interactions take place inside a magnetic shield in the presence of a well-defined internal longitudinal magnetic field (section 3.2).

3.1. Preparation of the cold atomic cloud

The key scientific achievement which enabled the operation of an atomic fountain was that of laser cooling. A historical review of the development of this technique is given in the 1997 Nobel lectures [28–30]. Here, the principles are recalled only briefly, insofar as their understanding is needed for the explanation of the operation of the atomic fountain clock.

First of all, a source of caesium atoms is needed. Traditionally it consists of a temperature-controlled caesium reservoir separated from the cooling chamber by a valve. The reservoir is held at a suitable temperature near room temperature in order to obtain a caesium partial pressure of the order of 10^{-6} Pa in the cooling chamber.

To obtain the required low temperatures of the atom samples in an atomic fountain the atoms are cooled in a

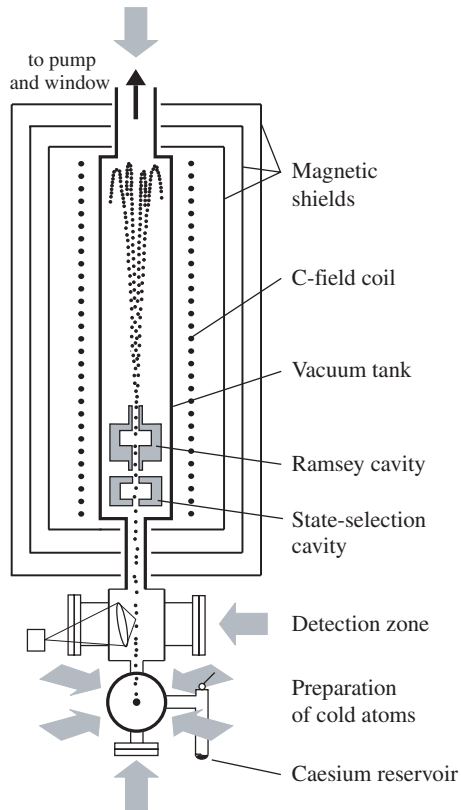


Figure 3. Simplified set-up of the atomic fountain clock

magneto-optical trap (MOT) [31] and/or an optical molasses (OM) [32, 33]. Common to both configurations is a set-up consisting of three mutually orthogonal pairs of counterpropagating laser beams, which are well balanced with respect to their intensities and usually have diameters of about two centimetres. So far two different laser beam geometries have been used. The first one uses two vertical, upward and downward directed beams (z -axis) and four horizontal beams, counterpropagating along the x -axis and the y -axis of a Cartesian coordinate system, respectively. This set-up offers the advantage of easy alignment but has the disadvantage that one pair of laser beams overlaps the atomic trajectories. These two laser beams are limited in diameter by the apertures (of typically 1 cm diameter) of the microwave cavity and are particularly critical in connection with laser light shift, i.e. an uncontrolled frequency shifting interaction with the atoms during their ballistic flight. These disadvantages are circumvented by the so-called '(1, 1, 1)' laser beam configuration, consisting again of three orthogonal pairs of counterpropagating laser beams, but with a different spatial arrangement: when in the previously described set-up the laser beams are imagined to run along the six face normals of a cube lying on one of its faces, in the (1, 1, 1) configuration this cube is balanced on one of its corners. Three laser beams (arranged symmetrically around the vertical axis) are therefore pointing downwards at an angle of 54.7° to the vertical and, accordingly, three laser beams are pointing upwards.

In figure 4 a simplified ^{133}Cs energy level diagram is shown. The frequency ν_c of the six cooling laser beams is tuned $2\Gamma-3\Gamma$ ($\Gamma = 5.3\text{ MHz}$, natural transition linewidth)

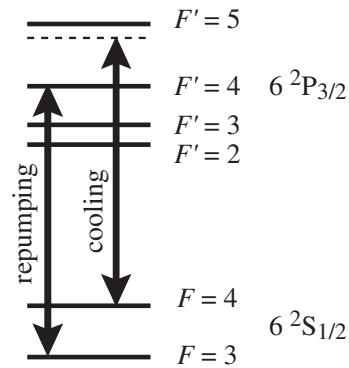


Figure 4. Simplified ^{133}Cs energy level diagram (not to scale) showing the hyperfine splitting of the $6^2\text{S}_{1/2}$ ground state and the $6^2\text{P}_{3/2}$ excited state. The excitation lines for cooling and repumping, respectively, are indicated by arrows.

to the red (low-frequency) side of the cyclic $|F=4\rangle \rightarrow |F'=5\rangle$ caesium transition in order to scatter a large number of photons before the atoms are eventually pumped into the other caesium hyperfine ground state $|F=3\rangle$. Although forbidden by selection rules, this hyperfine pumping process will happen in practice owing to small polarization imperfections in connection with off-resonant excitation to the excited state $|F'=4\rangle$. A repumping laser beam tuned to the caesium transition $|F=3\rangle \rightarrow |F'=4\rangle$ is therefore superimposed on at least one of the six cooling laser beams. It depletes the $|F=3\rangle$ level so that all atoms can continue to participate in the cooling process.

There exists a large variety of optical set-ups for providing all the necessary laser beams for fountain clock operation and here is clearly not the place to discuss them in detail. Generally speaking, such a set-up has to provide enough power for the six cooling laser beams in order to obtain for each beam an intensity of at least several mW cm^{-2} . Additionally, a few mW cm^{-2} intensity of repumping light is needed for the cooling region. For the detection region (see below) a few mW cm^{-2} of light intensity for the $|F=4\rangle \rightarrow |F'=5\rangle$ caesium transition and a very low intensity repumping laser beam are needed. Laser linewidths of a few megahertz are sufficient for cooling and repumping but the detection laser linewidth should be at most a few hundred kilohertz because otherwise there will be too much noise on the detected number of atoms to achieve a good short-term stability of the fountain clock [34].

The optical set-up has to provide the means of changing the laser light power and frequency in a precisely controlled way in order to properly cool, launch and detect the atoms. Finally, all the laser light has to be blocked completely during the interaction of the atoms with the microwave field in order to guarantee that the microwave transition frequency is not shifted by the ac Stark effect [35]. For reasons of compactness, low power consumption, reliability and ease of use most optical set-ups use exclusively laser diode systems. For details of the individual set-ups we refer to the relevant references (see, e.g., [15, 16, 22, 36, 37]).

Essentially two trapping configurations are employed in the existing fountains. One makes use of both an MOT and an OM phase while the other starts with an OM phase directly.

The working principle of an MOT relies on a differential excitation of magnetic ground state sublevels depending on the position of the atoms in the intersection region of the six cooling laser beams. This is accomplished by the combination of a spherical magnetic quadrupole field centred on the intersection region with circularly polarized cooling laser beams. The magnetic field gradient is usually generated by two coils operated in an anti-Helmholtz configuration. Typically, 10^7 – 10^8 atoms are trapped and cooled in a volume of about 1 mm^3 . The atom number is limited mainly by the available laser power and laser beam diameters.

During an initial MOT phase the number of trapped atoms increases quickly and then saturates with a time constant governed by the caesium partial pressure in the cooling region (and possibly the background pressure if it is not low enough). Typically, after a few tenths of a second, when enough atoms have been collected, the quadrupole field is switched off. This signals the beginning of the OM phase where the atoms are further cooled.

Afterwards the atoms are launched by the ‘moving molasses’ technique. The pattern formed by the interference of the trapping beams moving upwards and downwards can be made to move at a velocity $c\delta v/v_c$ when the upward-directed laser beam is tuned to a frequency $\nu_c + \delta v$ and the downward-directed laser beam to $\nu_c - \delta v$. In this upward-moving interference pattern the atoms are accelerated within milliseconds to velocities of several metres per second. As opposed to launching of the atoms by radiation pressure of the upward-directed beam alone, the atoms are heated much less by the moving molasses, which is essential for fountain operation.

The last cooling stage consists of a sub-Doppler cooling phase. In the absence of sub-Doppler cooling mechanisms the cloud temperature would be limited to $127 \mu\text{K}$ [38], the so-called Doppler limit. This is far too hot for a fountain clock to operate. So an optimized polarization gradient cooling phase [39,40] is implemented, during which the intensity of the cooling lasers is ramped down within a millisecond to about 0.5 mW cm^{-2} , together with a simultaneous increase of the detuning (10Γ – 12Γ). Detailed descriptions and explanations of the sub-Doppler cooling processes involved can be found in [38]. When the lasers are finally switched off altogether the caesium atom temperature is about $1 \mu\text{K}$ to $2 \mu\text{K}$. The post-cooling is applied only after the launch of the atoms, as the obtainable acceleration is larger at high laser intensity and small detuning.

Skipping the MOT phase and starting with an OM for the preparation of a sample of cold atoms reduces the number of cooled atoms by roughly a factor of ten. In this case a so-called $\text{lin}\perp\text{lin}$ polarization configuration of the cooling laser beams is more efficient. This kind of cloud preparation offers several advantages. First, the atomic cloud is larger, filling the cooling laser beam intersection region, which considerably reduces the atomic density for the same number of atoms compared with a fountain operation using an MOT. Hence, the collisional frequency shift (section 4.2.9) is reduced. Second, the increased atomic cloud size results in a better filling of the aperture of the microwave cavity for the atoms on their way up, which in turn results in a better compensation of transverse cavity phase gradients as they cancel out more completely for

a more homogeneous trajectory distribution. Third, the atomic cloud size does not depend on the number of atoms loaded (as it generally does in an MOT), thus removing a complication in the determination of the collisional frequency shift [41].

A compromise has been chosen for the operation of IEN-CsF1, in which after the MOT phase a free expansion–recapture sequence lowers the initial cloud density [15]. Here, the cooling laser beams are alternately switched on and off, taking advantage of the relatively high temperature of the atoms before the sub-Doppler cooling phase, in order to expand the atomic cloud.

In another approach a sequence of alternately switching off the vertical and horizontal cooling laser beams is used to heat the atoms which had been captured in an MOT before, again in order to extend the atomic cloud before the final polarization gradient cooling phase [22].

Since at the end of the post-cooling phase the repumping laser is switched off slightly later than the cooling laser, the atoms end up distributed among the atomic substates $|4, m_F\rangle$, where $m_F = -4, -3, \dots, +4$ indicates the magnetic substate. As the next step, a further state selection process can be applied to the atoms in order to reduce the background signal and the collisional shift due to atoms in states with $m_F \neq 0$ which do not take part in the ‘clock transition’ $|4, m_F = 0\rangle \rightarrow |3, m_F = 0\rangle$. This removal of atoms with $m_F \neq 0$ is a big advantage for fountain clocks over thermal beam clocks also because it reduces effects like the Rabi and Ramsey pulling and Majorana transitions [1]. For the state selection the $|4, m_F = 0\rangle$ atoms are first transferred by a microwave π pulse using the clock transition to the state $|3, m_F = 0\rangle$. This is often done in a microwave state selection cavity through which the atoms pass before they enter the Ramsey cavity for the first time. Afterwards, all the atoms which remained in the $|F = 4\rangle$ state are pushed away by a laser beam tuned to the $|F = 4\rangle \rightarrow |F' = 5\rangle$ transition, which is either pointing downward or is horizontal. This results in an atomic sample of atoms all in state $|3, m_F = 0\rangle$ entering the Ramsey cavity, where subsequently the clock transition $|3, m_F = 0\rangle \rightarrow |4, m_F = 0\rangle$ is excited.

3.2. Microwave interaction

One of the most critical parts of a fountain clock is the microwave cavity for the Ramsey interaction, through which the atoms pass twice, once on their way up and again on their way down. Much work has been done on different realizations of these delicate devices (see, e.g., [42–45]).

Obviously, there is no end-to-end cavity phase shift in a fountain clock, unlike the situation in a thermal beam clock [1, 2]. However, as the atomic cloud spreads during its ballistic flight, the atoms will, in general, cross the microwave field in the cavity at different positions on their ways up and down. In order to minimize the effect of transverse phase variations on the atomic transition frequency, cylindrical microwave cavities with the field oscillating in the TE_{011} mode have been used in fountain clocks (see, e.g., [15, 16, 36, 37, 46]). This mode (indicated in figure 5) exhibits particularly low losses (high intrinsic quality factor Q), which results in a particularly small running-wave component in the cavity. The dependence of the microwave phase on the transverse position

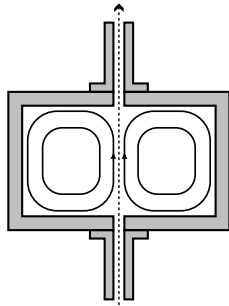


Figure 5. Sketch of the microwave field geometry inside a typical TE_{011} fountain cavity. Dotted line: trajectory of the atoms.

of the atomic trajectory is therefore also small. For a further reduction of the position dependence it is necessary to feed the microwave power symmetrically into the cavity so that microwave phase gradients are cancelled to first order. So far, feeding by two [16, 36, 46] and four ports [15, 37] have been realized. Up to now the uncertainty contributions arising from the transverse phase variations in the above-mentioned cavity realizations are estimated to be at the level of a few 10^{-16} or less.

The microwave signal feeding the cavity for probing the atomic transition is either synthesized from a low-noise BVA quartz-crystal oscillator or from a cryogenic-sapphire oscillator (CSO) [17], the latter exhibiting extraordinary frequency instability around 10^{-15} up to 800 s, before a slow drift sets in [46]. For the operation of most of the fountains the voltage-controlled oscillator (VCO) or the CSO is weakly phase-locked to a hydrogen maser which serves as a frequency reference for the fountain clock. By proper multiplication and mixing of the VCO (or the CSO) frequency with the frequency of a (usually commercial) synthesizer the 9.2 GHz microwave signal for the interrogation is generated. By square-wave modulation of the synthesizer output frequency from shot to shot of the fountain cycle, the atoms are probed alternately on the left and right sides of the central Ramsey fringe (inset of figure 2). The two transition probabilities for each side are subsequently compared and if they are not equal the synthesizer frequency is corrected. In this case the series of correction values gives the relative frequency difference between the fountain and the frequency reference.

Alternatively, the fountain output signal, i.e. the difference between the transition probabilities at both sides of the central Ramsey fringe, can be used directly to control the frequency of a VCO in a servo-loop, as described in [36]. In this case the VCO directly represents the fountain frequency and the VCO frequency has to be measured against an external frequency reference in order to obtain the relative frequency difference between the fountain and its reference.

In any case the measured fountain frequency differs from the unperturbed caesium transition frequency $\nu_0 = 9192\,631\,770$ Hz by the sum of all systematic frequency shifts. Usually this difference is of the order of 1 mHz (for comparison, the correction amounts to about 2 Hz in the case of CS2, a thermal beam primary standard) and its exact evaluation and the determination of its corresponding systematic uncertainty are the main difficulties encountered when a fountain is operated as a primary clock.

As in conventional caesium clocks, for the definition of a quantization axis and for removing the degeneracy of the magnetic substates, a magnetic ‘C-field’ is applied along the interaction region, that is from the Ramsey cavity region up to the apogee of the atomic ballistic flight. In order to ensure a C-field of high homogeneity the C-field is generated by a long, highly uniformly wound coil surrounded by multiple layers of a high-permeability magnetic shield. Owing to the long interaction time in fountain clocks, the Rabi envelopes of the microwave transition patterns are much narrower than in conventional caesium beam clocks. For this reason the C-field strength can be chosen to be much lower and is usually in the range of only a few hundred nanoteslas.

3.3. Detection and servo system

In a fountain clock the detection of the atoms is performed via the fluorescence light of the atoms which have passed the Ramsey cavity twice. Generally, both kinds of atoms, those in $|F = 4\rangle$ and those in $|F = 3\rangle$, are detected separately.

The usual detection set-up consists of three horizontal laser beams. When the falling atoms pass through a first transverse standing-wave light field tuned to the $|F = 4\rangle \rightarrow |F' = 5\rangle$ transition the fluorescence photons emitted by the atoms in the $|F = 4\rangle$ state are imaged onto a photodiode. The time-integrated photodetector signal, N_4 , is proportional to the number of atoms in the state $|F = 4\rangle$. From the shape of the time-dependent photodetector signal one can infer the axial velocity spread of the atoms in the cloud, which indicates the corresponding kinetic temperature. The $|F = 4\rangle$ atoms are then pushed away by a transverse travelling wave field tuned to the $|F = 4\rangle \rightarrow |F' = 5\rangle$ transition. Only the atoms in the state $|F = 3\rangle$ remain. These are then pumped to the state $|F = 4\rangle$ by a second horizontal detection laser beam, positioned slightly below the first and tuned to the $|F = 3\rangle \rightarrow |F' = 4\rangle$ transition. Depending on fountain design, this second laser beam can be spatially separate from or superimposed onto the third horizontal detection laser beam, which is again tuned to the $|F = 4\rangle \rightarrow |F' = 5\rangle$ transition. By the combined interaction with the second and third detection laser beams the atoms are thus first pumped to the state $|F = 4\rangle$ and are then detected by their fluorescence on the $|F = 4\rangle \rightarrow |F' = 5\rangle$ transition with the help of a second photodetector, giving a measure N_3 for the number of atoms that arrived in the detection zone in the state $|F = 3\rangle$.

In the servo system the ratio $N = N_4/(N_3 + N_4)$ is calculated. This ratio N is independent of the shot-to-shot fluctuations in atom number, which typically lie around 1%, and is used as the input signal to the microwave-frequency servo loop.

4. Uncertainty budget

4.1. Statistical (type A) uncertainties

Generally, in an atomic clock, several statistical uncertainty contributions sum up to a total statistical uncertainty u_A . Usually, the important noise contributions are well characterized by white noise processes. In this case a reasonable description of the statistical uncertainty obtained after a

measurement time τ is given by an Allan standard deviation $\sigma_y(\tau)$ which is proportional to $\tau^{-1/2}$ [47].

In a well-designed fountain clock the following noise contributions have to be considered [48]:

- (a) quantum projection noise [49]: resulting from the fact that a fountain clock is operated alternately on the left and right sides of the central Ramsey fringe where the transition probability is neither 0 nor 1;
- (b) photon shot noise: resulting from the statistical detection of a large number of photons per atom;
- (c) electronic detection noise: resulting from the electronic detection process by, typically, a photodetector in combination with a transimpedance amplifier;
- (d) local oscillator noise: resulting from a downconversion process of local oscillator frequency noise components because of the non-continuous probing of the atomic transition frequency in a pulsed fountain ('Dick effect') [50–53].

Based on the consideration of these noise contributions, the relative frequency instability expressed by the Allan standard deviation can be written as [48]

$$\sigma_y(\tau) = \frac{1}{\pi Q_{\text{at}}} \sqrt{\frac{T_c}{\tau}} \left(\frac{1}{N_{\text{at}}} + \frac{1}{N_{\text{at}} \epsilon_c n_{\text{ph}}} + \frac{2\sigma_{\delta N}^2}{N_{\text{at}}^2} + \gamma \right)^{1/2}. \quad (1)$$

In equation (1) τ is the measurement time in seconds, T_c the fountain cycle duration and $\tau > T_c$, $Q_{\text{at}} = \nu_0/\Delta\nu$ is the atomic quality factor with $\Delta\nu$ the width of the Ramsey fringe and ν_0 the caesium hyperfine frequency. N_{at} is the number of detected atoms, n_{ph} the average number of photons scattered per atom during detection and ϵ_c is the photon collection efficiency. $\sigma_{\delta N}^2$ is the uncorrelated rms fluctuation of the atom number per detection channel. The first term in the brackets of equation (1) indicates the atomic projection noise, the second the photon shot-noise of the detection fluorescence pulses and the third the noise of the detection system. Finally, γ is the contribution of the frequency noise of the local oscillator.

When detecting high numbers of photons per atom and using state-of-the-art low-noise electronic components, the noise contributions (b) and (c) can be reduced to such a level that the noise sources (a) and (d) remain as the dominant contributions. It can be seen from equation (1) that in this case a sufficiently high atom number results in a frequency instability limited by the noise spectrum of the local oscillator. With the best currently available VCOs the relative frequency instability is thus limited for typical fountain duty cycles to the order of $10^{-13}(\tau/\text{s})^{-1/2}$. A much better frequency instability of a fountain in the low $10^{-14}(\tau/\text{s})^{-1/2}$ range was achieved by the use of a cryogenic sapphire oscillator [17, 46, 48]. In this way the quantum-projection noise-limited operation could be demonstrated because of the superior noise properties of the cryogenic oscillator [48].

It should be mentioned that the above considerations assume the use of a state selection process as described in section 3.1. Without a state selection process an additional noise source has to be considered: the partition noise because of the varying occupation of the magnetic substates, as described in [54].

Finally, it should be pointed out that a small frequency instability is indispensable for the evaluation of several

systematic uncertainty contributions at the level of 10^{-16} or below. This becomes apparent in the light of the fact that a $10^{-13}(\tau/\text{s})^{-1/2}$ instability still results in a 3.4×10^{-16} statistical uncertainty after one full day of measurement.

4.2. Systematic (type B) uncertainties

In a fountain clock the frequency-shifting physical phenomena are in principle very similar to those in a conventional caesium beam clock [1]. Detailed descriptions of these effects can be found in [55]. Here, we will just summarize them and indicate the main particularities of fountain clocks. Detailed discussions of the effects in individual fountain clocks are compiled in the published formal evaluations, for example in [15, 16, 36, 37, 46]. The exemplary uncertainties given in the following subsections have all to be considered as relative frequency uncertainties.

4.2.1. Second-order Zeeman effect. As in conventional caesium clocks [1], in a fountain clock too, the applied magnetic C-field results in a second-order shift of the clock's transition, which has to be corrected due to its large size relative to the overall uncertainty of the fountain clock. The C-field increases the clock transition frequency by $f_c = 0.0427 \text{ Hz}(B_C/\mu\text{T})^2$, where B_C is the magnetic flux density of the C-field, so that almost 5×10^{-14} relative frequency shift is obtained for the typical magnetic C-field strength of $0.1 \mu\text{T}$. The determination of the relative frequency correction and its uncertainty is based on experimental data of the mean C-field strength, its inhomogeneity and its temporal stability.

It is appropriate to determine the correction f_c by measuring the transition frequency f_Z of a first-order field-sensitive transition, usually the $|4, m_F = 1\rangle \rightarrow |3, m_F = 1\rangle$ transition. In contrast to a conventional beam clock, an atomic fountain provides the advantageous possibility of mapping the C-field by launching the atoms to different heights h and calculating from $f_Z(h)$ the magnetic flux density $B_C(h)$ along the atomic trajectories. This gives direct access to the homogeneity of the C-field [54].

4.2.2. Majorana transitions. Majorana transitions ($\Delta F = 0$, $\Delta m_F = \pm 1$) between the m_F substates within a hyperfine ground state ($|F = 4\rangle$ or $|F = 3\rangle$) can be induced near zero crossings of the magnetic field strength [56]. In real caesium clock cavities it cannot be avoided that due to the field geometry some $\Delta F = \pm 1$, $\Delta m_F = \pm 1$ transitions take place besides the designated clock transition, albeit with a small probability. In connection with Majorana transitions, large frequency shifts can occur [57] because atoms can get into superposition states with the same F quantum number but different m_F quantum numbers. For these states the hyperfine transition frequency is, in general, different from the clock transition frequency, with a resulting overall frequency shift. The uncertainty estimate due to Majorana transitions is typically quoted as well below 10^{-16} .

4.2.3. Cavity-related shifts: residual first-order Doppler effect and cavity pulling. A general advantage of an atomic fountain microwave frequency standard is that the atoms cross the same microwave cavity twice. If the atomic trajectories

were perfectly vertical, frequency shifts due to axial and radial cavity phase variations would be perfectly cancelled as each atom would interact with the field once with velocity v (upwards) and once later with $-v$ (downwards). It is the transverse residual thermal velocity and a possible misalignment of the launching direction that cause a spread of the trajectories between the first and the second passages through the cavity. In this case, a non-vanishing transverse phase variation of the cavity field can give rise to a residual first-order Doppler frequency shift, unless the trajectories happen to be distributed around the vertical symmetry axis in a favourable way.

Current cavities of evaluated fountain clocks are estimated to exhibit uncertainty contributions of at most several 10^{-16} arising from transverse phase variations [15, 16, 36, 37, 46]. Sometimes these uncertainty estimates are the result of worst-case considerations and might be reduced in the future.

Usually in an atomic fountain the atom number and the loaded quality factor of the cavity are such that the operating conditions are far from maser oscillation [55]. Therefore, at low cavity detuning and optimum microwave excitation, the frequency shift due to cavity pulling is usually negligible, according to equation (5.6.123) of [55]. Since cavity pulling is proportional to atom number it is corrected for automatically when the collisional shift correction (see section 6) is applied.

4.2.4. Rabi and Ramsey frequency pulling. Frequency shifts due to Rabi and Ramsey frequency pulling [1] can occur in the presence of non-zero and asymmetric (with respect to $m_F = 0$) populations of the $|F, m_F \neq 0\rangle$ substates when the atoms enter the Ramsey cavity. Generally, the state selection process (see section 3.1) in a fountain clock strongly reduces the impact of these frequency pulling effects to well below 10^{-16} .

4.2.5. Microwave leakage. The effect of microwave leakage [1] due to the exposure of the atoms to a residual travelling microwave field outside the cavity is again somewhat reduced in a fountain clock when compared with conventional beam clocks because of the almost symmetrical trajectories of the atoms going up with the same but opposite velocity with which they fall down. However, as there is no perfect symmetry also in a fountain clock, microwave leakage can be of concern and its possible effect has to be carefully analysed. Typical uncertainties evaluated so far fall in the low 10^{-16} range.

4.2.6. Electronics and microwave spectral impurities. The frequency shifting effects due to the electronics and to microwave spectral impurities are essentially the same in a fountain clock and in a conventional beam clock so that we refer here to [1]. However, the lower total systematic uncertainties of fountain clocks set much tighter limits on the performance characteristics of the microwave synthesis devices used for the operation of these fountain clocks.

4.2.7. Light shift. The interaction of atoms with laser light during the ballistic flight in and above the microwave cavity entails a frequency shift through the ac Stark effect (light shift) [35]. To prevent this effect, usually the laser light

is blocked by mechanical shutters. As an added precaution, the laser light frequency can be far detuned during this phase of fountain operation. By intentionally increasing and measuring the effect and by effective controls of the shutter action, the corresponding uncertainty can typically be reduced, at least, to the very low 10^{-16} region.

4.2.8. Blackbody shift. During their microwave interaction (including the ballistic flight above the Ramsey cavity) the atoms are subjected to thermal radiation of the vacuum enclosure. If this radiation gives rise to a spectral power density distribution which is equivalent to that of a black body, according to [58, 59], the clock transition frequency is shifted by

$$f_{\text{bb}} = -1.573(3) \times 10^{-4} \text{ Hz} \left(\frac{T}{300 \text{ K}} \right)^4 \times \left[1 + 0.014 \left(\frac{T}{300 \text{ K}} \right)^2 \right] \quad (2)$$

for a vacuum enclosure at temperature T . Hence, for a caesium clock at room temperature the relative frequency shift is of the order of -17×10^{-15} .

The first numeric coefficient in equation (2), $K_{\text{Stark}} = -1.573(3) \times 10^{-4}$ Hz, is a result of a dc electric Stark shift measurement performed with a caesium fountain in Paris [59]. The uncertainty of this value of K_{Stark} itself is not likely to become a limiting factor for fountain clocks operated near room temperature or slightly above.

A confirmation of equation (2) was obtained earlier in a true ac electric Stark shift measurement by varying the temperature of a conventional caesium beam clock at PTB [60–62]. However, the uncertainty of K_{Stark} obtained in the PTB experiment was significantly larger. Recently K_{Stark} was remeasured using atomic caesium fountain clocks and differing results were obtained. While an Italian group obtained experimental and theoretical values of K_{Stark} consistent with each other but differing from the values indicated in equation (2) [63, 64], a new measurement with a fountain in Paris confirmed the old value [65]. Moreover, another recent theoretical evaluation claims to confirm the former value as well [66]. The current, somewhat unclear, situation is illustrated in figure 6, where the published experimental and theoretical results for K_{Stark} are compiled. A clear solution of this problem would be highly desirable because the black-body shift is a large correction compared with the uncertainty of a fountain clock.

4.2.9. Collisional shift. A major source of uncertainty is the frequency shift due to collisions among the cold atoms in the cloud [72]. The collisional cross-section was found to be strongly dependent on energy (i.e. the average temperature of the cloud) [73]. The problem is particularly serious for caesium because it was found that its collisional cross-section is unusually large at the low cloud temperatures used in a fountain. Conceptually, the simplest solution would be to choose another element. For instance, in rubidium the collisional cross-section is almost two orders of magnitude lower [74]. Indeed, rubidium fountain clocks have been built where the reduction of collisional shift uncertainty was one

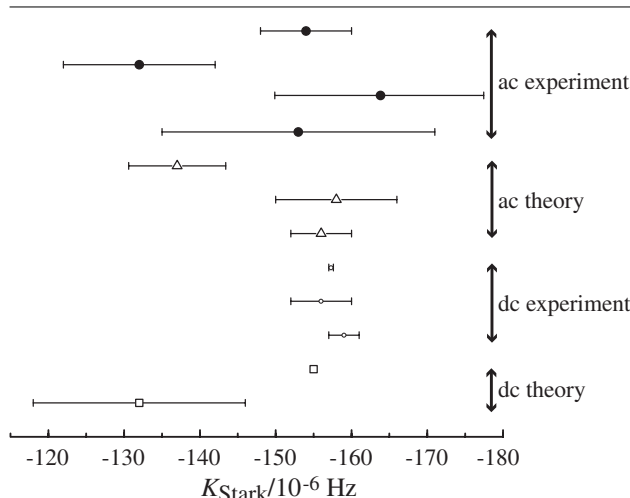


Figure 6. Theoretical and experimental values of the black-body shift coefficient K_{Stark} over the course of time. Figure adapted from [65]. The data points are extracted, from bottom to top, from [67, 68, 69, 70, 59, 58, 71, 64, 60, 61, 63, 65].

of the motivations. Rubidium fountain clocks will be treated below (section 7).

A number of schemes have been devised to reduce the collisional shift or at least its contribution to the uncertainty budget of the caesium fountain clock. These will be discussed in more detail in section 6. We should also note that the experimental signatures of cold collision shift and cavity pulling are very similar, something that can be used to partially tune the overall effect away when the isotope-specific relative shift rates happen to be suitable, as in the case of ^{87}Rb [75].

4.2.10. Background gas collisions. Contrary to the effect of cold collisions between the caesium atoms, the effect of residual gas collisions in fountain clocks is estimated to be well below 10^{-16} as typical vacuum pressures in the ballistic flight region are at most in the low 10^{-7} Pa range.

4.2.11. Time dilation: relativistic Doppler effect. Special relativity predicts that owing to time dilation the clock frequency observed in the laboratory frame is reduced by $f_{\text{D}} \approx \nu_0 \langle v^2 \rangle / (2c^2)$, with $\langle v^2 \rangle$ the mean quadratic velocity of the atoms above the microwave cavity and c the velocity of light. Typically, in a fountain clock f_{D}/ν_0 is of the order of 10^{-17} , so that in contrast to thermal beam clocks time dilation and the associated uncertainty contribution can be neglected.

4.2.12. Gravitational redshift. Finally, it should be mentioned that even though the gravitational redshift [1] is not relevant for the realization of the *proper* second of a clock, its knowledge is necessary for comparing remote clocks and for contributing to international atomic time (TAI). Hence the mean height of the atoms above the geoid during their ballistic flight above the microwave cavity centre has to be determined with a typical uncertainty of 1 m, corresponding to a frequency uncertainty of 10^{-16} . In principle, a limitation is given by the accuracy with which the local gravitational potential can be determined. Even for high-altitude laboratories like NIST in Boulder (≈ 1630 m above sea level) the correction can be

determined with a relative uncertainty of 3×10^{-17} [76]. At this relative uncertainty the gravitational redshift will probably not become a limiting factor for clocks based on microwave transitions.

4.2.13. Summary of systematic effects. There are other frequency shifting effects (dc Stark shift, Bloch–Siegert shift [1]), which can be estimated to be less than 10^{-17} in a fountain clock. In conclusion, it can be stated that the main contributions to systematic uncertainty are of the order of a few 10^{-16} or less. As the individual systematic uncertainty contributions can be assumed to be independent, the resulting total systematic uncertainty is the square root of the sum of squares of the individual contributions. Specific examples are presented in section 8 in connection with the state-of-the-art in fountain clocks.

5. Fighting the Dick effect

A serious limitation of the short-term stability of an atomic fountain clock is given by the phase noise of the local oscillator from which the 9 GHz signal is derived. Any phase excursions of this oscillator, while no atoms are in or above the microwave cavity, will go undetected and therefore add some of the phase noise of the local oscillator to the output of the clock. A quantitative description of the Dick effect is beyond the scope of this review; it can be found in [50–53].

We will now discuss recently developed ways of reducing the influence of the Dick effect. One can use a better local oscillator or reduce the dead time of the fountain, i.e. by launching the next cloud as quickly as possible after the previous one. However, some dead time is unavoidable in a standard pulsed fountain because one has to wait until the detection process is finished before the next cloud can be launched. A continuous-beam fountain clock, however, would be practically immune from the Dick effect.

5.1. High-stability cryogenic oscillator

Conceptually, the easiest way to reduce the influence of the Dick effect on the short-term instability is to use a more stable local oscillator. Using a cryogenic sapphire oscillator developed at the University of Western Australia [77] and a specially designed low-noise microwave synthesis chain, the group at SYRTE was able to reach a fractional frequency instability of just $1.6 \times 10^{-14} (\tau/\text{s})^{-1/2}$ [46], which was only limited by quantum projection noise [48].

Let us note here that there have been proposals to use spin-squeezed atomic samples in order to lower the projection-noise limit [78]. Today it appears, however, as if these schemes, devised with idealized conditions in mind, would be difficult to transfer to an actual clock.

Despite the additional effort of liquid helium refrigeration required for low-noise cryogenic sapphire oscillators, today several metrology laboratories worldwide are developing such systems. It will be interesting to see whether designs based on closed-cycle coolers [79] rather than liquid helium refrigeration can, one day, deliver the performance needed for state-of-the-art fountain clocks.

5.2. Loading from an atomic beam

Another strategy for reducing the influence of the Dick effect is to speed up the loading and preparation of the cold atomic cloud, in order to reduce the fraction of the fountain cycle where no atoms are in or above the microwave cavity. MOT or molasses loading times can be greatly shortened when the atoms are collected not from the residual background vapour but from a slow atomic beam. For instance, both FO1 and FO2 are equipped [17] with a chirp-slowed atomic beam [80]. Typically, for the same loading time, a molasses loaded from a slow beam captures more than ten times as many atoms as a molasses loaded from the background vapour.

In the case of FO2 the slow atomic beam is, in addition, transversely collimated by a two-dimensional OM [17, 81]. Not only does the transverse collimation reduce the background pressure of atoms in the preparation zone but it also prolongs the useful life of one filling of the oven because the same atomic flux can be obtained with a lower oven temperature. For instance, in the case of FO2, the collimation alone has reduced the capture time from 900 ms to 300 ms and increased approximately ten-fold the lifetime of one caesium charge [81].

Loading from a slow beam is indispensable when implementing a multi-toss scheme, see section 6.1. By choosing a suitable mode of operation, dead times can also be greatly reduced by this approach.

5.3. The continuous fountain clock

The Dick effect can be all but eliminated when the fountain clock is operated in a continuous mode rather than pulsed [82]. At the same time, because of the continuous detection, a lower-density beam can be used, reducing the uncertainty due to cold collisions. Development of such a fountain was undertaken at the Observatoire Cantonal in Neuchâtel/Switzerland [18]. Design goals have a relative short-term instability of $7 \times 10^{-14} (\tau/s)^{-1/2}$ (using a quartz oscillator as a local oscillator for the 9 GHz synthesis chain) and a relative uncertainty of 10^{-15} .

A continuous fountain poses a number of technical and experimental challenges. First of all, since the preparation and the detection zones have to be spatially distinct, the atoms have to fly along a parabolic path (figure 7). This requires a special geometry for the main cavity (figure 8). Unfortunately, in this way one loses one of the big advantages of the pulsed fountain design, where the atoms retrace their path through the microwave field and thus mostly cancel any end-to-end phase shifts in the cavity. In the continuous fountain a special device allows one to rotate the cavity around the vertical axis by precisely 180° , so that an effective beam reversal occurs [83], in analogy to the procedure in thermal beam clocks [2].

The openings in the cavity for the atomic beam fix the geometry of the parabolic trajectory, so that only one toss-height is possible—making, for instance, the characterization of the magnetic field inhomogeneity more difficult than in the pulsed case. And finally, the suppression of stray light from the preparation zone becomes more complicated. Unlike in the pulsed case, the laser light cannot be switched off during the free-flight phase of the atoms, hence for the continuous

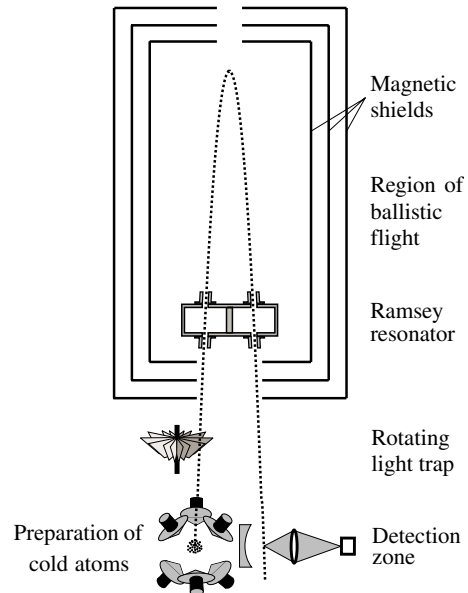


Figure 7. Sketch of the vacuum subsystem of the continuous fountain clock at METAS/Switzerland [83]

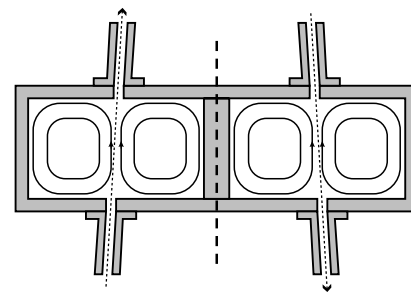


Figure 8. Microwave cavity and mode geometry of a continuous fountain clock [18]. The dotted line indicates the trajectory of the atoms, the dashed line the axis of rotation for beam reversal.

fountain one resorts to mechanical shutters inside the vacuum vessel. A wheel with partially overlapping filters absorbing the laser radiation rotates rapidly through the atomic beam in such a way that the direct line of sight from the detection zone into the free-flight zone passes through at least one filter at any one time. Not only does this chop thin slices out of the continuous atomic beam but also one needs to have a motor inside the ultra-high vacuum system—which in addition has to be non-magnetic!

Details of all design issues can be found in the thesis by Joyet [83]. Ramsey fringes 1 Hz wide have been seen with the Neuchâtel continuous fountain clock before it was transferred to METAS in Bern/Switzerland [18], where it is currently in the process of being made operational.

For a second continuous fountain in Neuchâtel a Raman sideband cooling technique is under development [84, 85] in order to improve the collimation of the continuous beam and therefore increase the atomic flux reaching the detection zone [86]. This technique may also be useful for pulsed fountains to enable reduction in the atom density (i.e. the collisional shift) while at the same time keeping the number of detected atoms the same (i.e. signal-to-noise ratio).

6. Fighting the collisional shift

Traditionally, one of the dominating systematic uncertainties of a fountain clock is due to the collisions of the cold atoms within the cloud, as explained earlier (section 4.2.9). In principle, it is easy to reduce this uncertainty by reducing the density of the atomic cloud and therefore the collision rate. A reduced number of atoms, however, reduces the detected signal amplitude and therefore the signal-to-noise ratio and the short-term stability (equation (1)).

Recent developments help to ease this trade-off problem in the case of caesium. The problem of loss of signal for low-density clouds can be circumvented by controlling the preparation of the atoms such that more than one cloud at a time travels through the vacuum system. We will present these ideas first, before covering the extrapolation methods, where the clock's output frequency is measured for two or more effective densities of the atomic cloud and then extrapolated to zero density. As discussed above, the continuous fountain also allows one to reduce the influence of collisional shift.

6.1. Multi-cloud fountains

One way of decreasing the collisional shift without reducing the number of detected atoms is to have several atomic clouds of correspondingly lower atom number and density travelling inside the vacuum tube at any time. Two realizations of this idea have been proposed.

The first is called the 'juggling fountain' [87]. Just like a human juggler keeps several balls in the air simultaneously, some of them going up while others come down, one can keep launching atomic clouds with a time separation smaller than the flight time of an individual cloud. Since each cloud is less dense than in the standard single-cloud case the internal collision rate is reduced as desired. However, the individual 'balls' penetrate each other in free flight, which could in principle give rise to additional collisions. The clever trick in the juggling fountain is to choose the timing and launch velocities of the individual clouds such that each time two of them meet their relative energies fulfil the condition for a Ramsauer resonance. As a consequence, they fly through each other basically without scattering, i.e. without additional collisional shifts. It is straightforward to do this with just two 'balls', but amazingly it can also be done with more than two balls [88].

However, the multi-ball scheme requires a precise control of the launch times, velocities and densities of the individual balls. Furthermore, it relies on a delicate cancellation of the collisional shifts in successive two-ball collisions, making use of the energy dependence of sign and amplitude of the shift [88].

A more robust multi-ball scheme has been proposed by Levi *et al* [89]. Once again several balls (up to ten or so) are launched in quick succession but with successively decreasing launch heights (figure 9). These balls never meet in the free-flight zone above the cavity where collisions would lead to a frequency shift. But they all come together in the detection zone—where cold collisions no longer matter—to produce a strong signal.

Since the later balls spend less time above the cavity the overall Ramsey pattern is a superposition of one pattern for

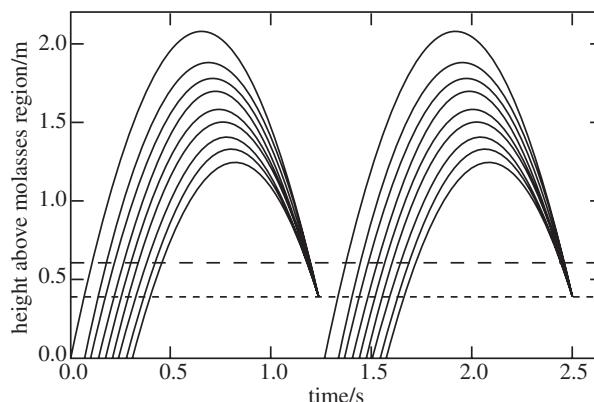


Figure 9. Trajectories of the multiple atomic clouds in the multi-toss scheme. The upper dashed line denotes the position of the cavity, the lower one that of the detection zone. Figure adapted from [90].

each ball, each of those having a different fringe spacing. In principle, this leads to a small broadening of the central Ramsey fringe. In the example calculated in [89] the fringe width increases only by 18%. On the other hand, the detected signal increases because all balls are loaded during the initial, steep part of the MOT loading curve [89]. A technical disadvantage is that a fast, mechanical shutter must be brought into the vacuum system in order to protect the balls that have already been launched from the stray light produced while cooling and launching the next balls. But once the shutter is present, it also allows loading of the first ball of the next sequence to commence while the balls of the previous sequence are still in flight, thus greatly reducing the dead time [90]. Preliminary tests of this scheme with up to seven balls have been performed at NIST [90]. Further consideration is needed regarding the correction of systematic frequency shifts, which might be different for different balls in the sequence because of their different launch heights and travel times.

6.2. Extrapolation methods

Since the frequency shift due to cold collisions is linear in effective atom density, one can extrapolate the measured frequencies obtained with clouds of different densities to zero density using linear regression. This is the method currently employed by all primary fountain clocks. Since the actual density of the cloud is not readily accessible in the experiment, one substitutes the number N_{at} of detected atoms instead. This, of course, assumes that there is a strict proportionality between N_{at} and effective density. The actual experimental practice in the various laboratories differs in the way that clouds of different densities are prepared.

PTB's CSF1 is operated under optimum conditions during the whole frequency evaluation period. For about 10 days before and after such a period CSF1 is switched every day or every half-day between operation at the standard atom number N_{at} and operation at $5N_{\text{at}}$, where the latter is obtained by increasing the length of the initial MOT phase [36]. The length of the ≈ 10 -day epoch was chosen so that the instabilities of the local H-masers, which are used as frequency references, no longer play a role. A disadvantage of this method is that despite the expansion during the molasses phase one cannot

exclude a difference in the spatial distribution of the atoms within the cloud for the two atom number regimes, which, in general, could change the proportionality factor between effective density and detected atom number. An additional contribution is therefore included in the uncertainty budget.

At NPL's CsF1, the collisional shift is monitored during the course of a frequency evaluation by switching between two different atom numbers every few shots [16]. The switching is done by varying the microwave power or detuning for the state-selection pulse. Once again it cannot be excluded that the density distribution of the state-selected cloud changes between high and low atom number due to inhomogeneities of the microwave excitation.

For IEN-CsF1 the MOT loading parameters are changed to obtain two atom numbers differing by a factor of 3 [15]. Switching between the two regimes occurs on an hourly basis, a schedule chosen so that the drift of the local H-maser does not affect the measurement.

The procedure for NIST-F1 combines elements of the previously described ones. Cs pressure, molasses loading time and molasses laser power are adjusted to change the number of atoms launched upwards [91]. A servo loop slightly adjusts the microwave power in the selection cavity so as to keep the detected atom number constant. Owing to the availability of a very stable local timescale, AT1E, the collisional shift determination can be stretched over many days, with measurements at medium, high and again medium densities where each phase lasts for a few days. These are bracketed by 10-day measurements at low density. Because of the stable local time scale these two 10-day stretches can be stitched together into a 20-day run. Another specialty of NIST-F1 is that it is operated at very low density where the collisional shift itself is reduced—and with it the absolute uncertainty of that shift. The concomitant reduction in stability can be tolerated in view of the noise on the time-transfer link to other laboratories. All one needs to do is to make sure that at the end of the 20 days of effective measurement time the fountain instability has reached a level low enough not to limit the total uncertainty including the time-transfer uncertainty.

At SYRTE, fountain operation is switched back and forth between two different atom densities, first for about 50–100 shots at a detected atom number N_{at} and then at an atom number which is as precisely as possible equal to $N_{\text{at}}/2$, but without changing the density distribution or temperature of the cloud. The more precise the density ratio the better one can extrapolate to zero density. To this end a new technique of state preparation was developed at SYRTE, the adiabatic rapid passage method [92]. This method relies on the fact that the population of one atomic state can be transferred with 100% efficiency into another one when both frequency and amplitude of the microwave radiation inducing the transition are ramped with just the right timing [93]. Here, the two states in question are the initial state $|F = 4, m_F = 0\rangle$, in which the atoms arrive from the cooling zone, and the final state $|F = 3, m_F = 0\rangle$, in which they should enter the main microwave cavity.

We cannot go into the physical basis and the technical details of the technique here; these can be found in [81, 92, 93]. Briefly, one has to ensure that the rate of change of the microwave frequency has to be much lower at all times than the square of the Rabi frequency (which is proportional to

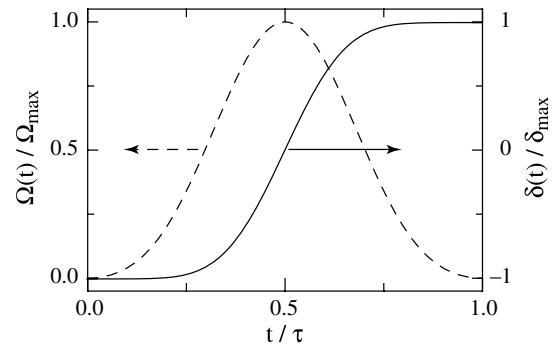


Figure 10. Dashed line: amplitude shape of the Blackman pulse of duration τ used in the adiabatic rapid passage method. Solid line: shape of the corresponding detuning curve.

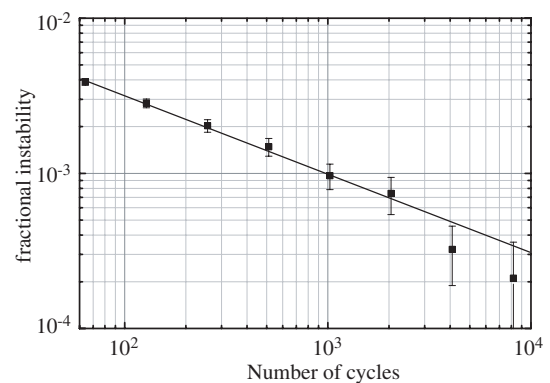


Figure 11. Fractional instability σ_R of the ratio R of detected atom number of low and high density configurations, as a function of the number of fountain cycles of ≈ 1.3 s each. Figure adapted from [46].

microwave power). At SYRTE this is realized by sending into the selection cavity a microwave pulse where the amplitude changes in time according to a Blackman shape (figure 10). This pulse shape is a compromise between pulse width and suppression of additional Fourier components in the microwave spectrum. The corresponding time behaviour of the detuning is also shown in figure 10.

When the pulse is switched off abruptly at detuning $\delta = 0$ the atoms are left in an exactly equal superposition of both states. The important feature of the rapid adiabatic passage is that this happens independently of the actual Rabi frequency an atom sees, i.e. it does not depend on where an atom passes through the field inside the cavity (the field amplitude decreases across the aperture when going away from the centre). The pushing beam therefore removes exactly half of all the atoms, without changing the density distribution, temperature or velocity of the cloud—in contrast to the other methods where such changes cannot be excluded.

At SYRTE the ratio of 1 : 2 can be prepared and maintained with an accuracy of 10^{-3} [46], allowing for a very precise determination of the collisional shift rate and its correction. Figure 11 gives an indication of the extraordinary temporal stability of the atom number ratio of 1 : 2. The precise control over atomic populations in SYRTE-FO2 has also made it possible to detect Feshbach resonances in the dependence of the collisional shift on magnetic quantum number m_F [94]. Surprisingly, these resonances occur already for flux densities of $2 \mu\text{T}$ or less.

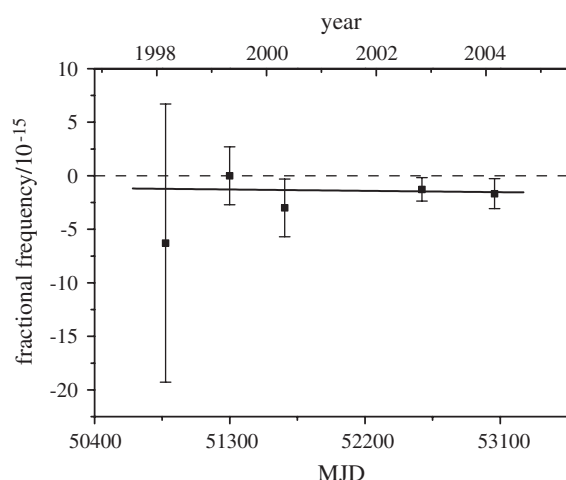


Figure 12. Hyperfine frequency of ^{87}Rb relative to that of ^{133}Cs as a function of time. The data point near MJD 51300 has been chosen as a frequency reference. The solid line is a regression line. Figure adapted from [46].

7. The rubidium fountain clock

There are several motivations for extending the fountain principle from caesium to rubidium. One is that it is always interesting to compare the behaviour of different atomic species under the same conditions or to use one as a reference for the other. In the case of atomic clocks this has a direct application in the search for a variation of fundamental constants of nature [95]. But one can also try to explore the limits, and the physics behind those limits, of the experimental technique itself. The more test candidates are available, the better the data base.

In the case of fountain clocks, rubidium is a natural candidate because the atomic physics is qualitatively similar to caesium and because laser cooling and manipulation are just as conveniently possible as with caesium. The set-up and the operation of a rubidium fountain clock are basically the same as those of a caesium fountain clock.

Even more interesting is that the cross-section for phase-changing collisions among cold ^{87}Rb atoms is much smaller than among cold caesium atoms. A factor of 15 was predicted theoretically [96]. In fact, this cross-section is so low that it was difficult to measure its value; initially only upper limits of 30 [75] or more than a factor of 50 [74] to the advantage of ^{87}Rb were published. Clearly, this has sparked quite some interest in Rb fountain clocks [97], and several are under construction in time laboratories around the world.

The most obvious thing to do with an Rb fountain is to measure its output frequency with respect to that of caesium. The first such measurement, using an early version of an Rb fountain at SYRTE, improved the accuracy about ten-thousand-fold over previous measurements and also, quite surprisingly, found a disagreement with the accepted literature value of more than 2 Hz [98]. When this measurement is repeated at later times (figure 12) one not only gets an indication of the reproducibility, but it is also possible to interpret the result in terms of the constancy of the constants of nature. In particular, the Rb–Cs comparison is sensitive to variations of the combination $\alpha^{0.44}\mu_{\text{Cs}}/\mu_{\text{Rb}}$, where α is the

fine structure constant and the μ are the nuclear magnetic moments [95]. It was found that the relative change of this combination (i.e. that of the frequency ratio $\nu_{\text{Cs}}/\nu_{\text{Rb}}$) over a time interval of five years is no larger than $7 \times 10^{-15} \text{ yr}^{-1}$. In the meantime, this value has been improved through another comparison in 2004, to $5.3 \times 10^{-15} \text{ yr}^{-1}$ [81].

Although this value is neither model-independent nor the most stringent limit on the variation of α at the present epoch (even when assuming $\mu_{\text{Cs}}/\mu_{\text{Rb}}$ to be constant), owing to its unique combination of constants it is nevertheless an important contribution to the search for time variations of the constants of nature.

The precise and repeated measurements of $\nu_{\text{Cs}}/\nu_{\text{Rb}}$ have led to the adoption of the hyperfine frequency $\nu_{\text{Rb}} = 6834\,682\,610.904\,324 \text{ Hz}$ of ^{87}Rb as a secondary representation of the second with a relative uncertainty of 3×10^{-15} [99]. The quoted uncertainty is about three times that of the actual measurement.

A substantial part of the uncertainty of the frequency ratio arises from the instability of the three fountain clocks employed in the measurements at SYRTE (FO2(Cs), FO2(Rb) and FOM), and from the unavoidable gaps in the frequency data. FO2 is actually equipped for simultaneous operation with Rb and Cs, although to date it has always been run with a single species only. The beginning of its operation with the simultaneous use of both alkalis is imminent. One can expect a reduced uncertainty in the Rb–Cs comparison when data taking is truly simultaneous. Furthermore, since Zeeman coefficients, polarizabilities and other atomic-physics quantities are different for the two atomic species one can correct partially for some of the systematic uncertainties in fountain clocks.

8. State of the art

In table 1 are collected the most recently published values of selected uncertainty contributions for the seven operational primary fountain clocks.

The superior stability of the fountains at SYRTE is largely due to the cryogenic sapphire oscillator available there. A series of improvements has allowed both SYRTE and NIST to reduce the relative uncertainty of their fountain clocks to well below 10^{-15} , with the other laboratories expected to follow suit.

It becomes apparent from table 1 that it will be difficult to drive the relative uncertainty much below 3×10^{-16} . On the one hand there appears to be room for substantial reduction in the uncertainties of collisional shift, cavity-related effects and electronics by a more stringent control of operating parameters and a better theoretical understanding of microwave cavities (gained perhaps along the lines of [101]).

On the other hand, reducing the uncertainty of the black-body shift appears rather difficult for the existing fountains because it would require a detailed knowledge of the effective thermal environment of the atoms during their free-flight phase. This includes not only the actual inner-wall temperature to within better than 1 K but also reliable values for the emissivity of the inner surfaces of the vacuum tube (which might change due to physisorption or chemisorption of caesium or residual gases over the years of operation) as well

Table 1. Some of the relative type-B uncertainty contributions (multiplied by a factor of 10^{16}) of the seven primary caesium fountain clocks. All values are based on the latest publications. The entry for ‘Total type-B’ includes other systematic effects not listed in the table. Note that in most cases the operating conditions for lowest systematic uncertainty are different from those needed to obtain the lowest instability.

Cause of frequency shift	SYRTE-FO1 ^a	SYRTE-FO2 ^b	SYRTE-FOM ^c	NIST-F1 ^d	PTB-CSF1 ^e	IEN-CsF1 ^f	NPL-CsF1 ^g
Cold collisions	2.4	2.0	5.8	1 ^h	7	12	8
Black-body radiation	2.5	2.5	2.5	2.6	2	0.7	4
Distributed cavity phase	<3	<3	<2	<0.3	5	<0.3	3
Electronics, microwave leakage	3.3	4.3	2.4	1.4	2	<2	3
Total type-B uncertainty ⁱ	7.2	6.5	7.7	3.3	9	16	10
Standard ⁱ instability at 1 s	410	280	1900	6000	2000	3000	4000

^a [17, 46], ^b [17], ^c [46, 81], ^d [37, 100], ^e [36], ^f [15], ^g [16], ^h treated by this group as a type-A uncertainty, ⁱ under the operating conditions for lowest uncertainty.

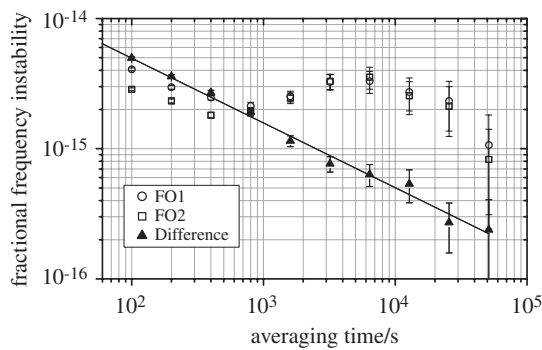


Figure 13. Allan standard deviation $\sigma_y(\tau)$ of the difference frequency of FO1 and FO2. Figure adapted from [46].

as the influence of radiation coming in through windows and other openings. However, any substantial progress on this front might require the cooling of the walls of the vacuum tube.

9. Comparing different fountain clocks

It is vital to compare the output frequencies of different fountain clocks as this provides a direct test for undiscovered systematic frequency shifts in an individual realization of the fountain clock. Unfortunately, at present SYRTE is the only laboratory having more than one working fountain clock. A recent comparison of FO1 and FO2 has given impressive results [46]. The relative instability of the difference frequency of the two fountains averages down nicely according to a white-noise law, reaching 2.2×10^{-16} for averaging times of 50 000 s (figure 13). At the same time, the average of the difference frequency of 4×10^{-16} is consistent with the stated inaccuracies of the two fountains.

In order to compare fountains in different laboratories one has to use a satellite frequency transfer technique. The first fountain frequency comparisons were performed between NIST-F1 and PTB-CSF1 at four epochs between August 2000 and February 2002 [102], finding agreement well within the uncertainty intervals of about $(2-3) \times 10^{-15}$. In the summer of 2003, FO2 and FOM in Paris and CSF1 at PTB were run simultaneously for a duration of 11 days [103]. Their frequencies were recorded relative to a local hydrogen maser. The maser frequencies in turn were compared using both common-view GPS and TWSTFT, thus permitting deduction of the relative frequency differences between the fountains (figure 14). The largest contribution to the length of the uncertainty bars for the CSF1 points originates from the

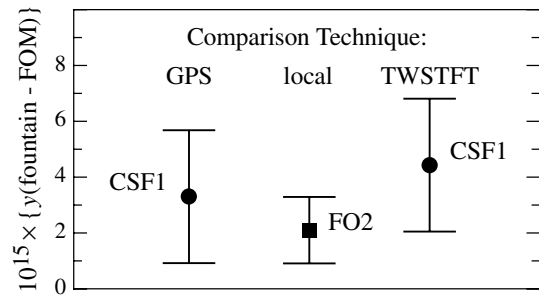


Figure 14. Frequency of CSF1 relative to FOM, as determined via GPS-common view and TWSTFT (●), and frequency of FO2 relative to FOM determined from a local comparison (■).

uncertainty of the satellite link. Given the overall uncertainty, all clock frequencies are consistent with each other. A similar experiment was performed at the end of 2004, involving SYRTE-FO2, NPL-CsF1 and IEN-CsF1 [104]. It was found that over the 20 days of joint data taking the relative frequencies of SYRTE-FO2 and NPL-CsF1 almost coincided whereas that of IEN-CsF1 lay about 4×10^{-15} higher, still consistent with the total uncertainty of 2×10^{-15} .

Another way of indirectly comparing fountain clocks in different laboratories is via the *Circular T* of BIPM. Apart from PTB's thermal clocks CS1 and CS2, which are operated continuously as primary standards, and occasional contributions by laser-pumped thermal beam standards at NICT/JP and at SYRTE, the bulk of the information needed for the steering of TAI is currently provided by fountain clocks (figure 15).

After a long pause, following the initial reports of FO1's frequency by the Paris group, both NIST-F1 and PTB-CSF1 started to report regularly to BIPM. The good agreement between the data points of these two fountains is an indication that the uncertainties claimed at the time were not unrealistic. As more and more fountain clocks became operational the density of reports has increased. The scatter, introduced by a few early data points with large uncertainty, has become smaller now that the reported uncertainties have become smaller.

10. Other applications

The same ideas used in fountain clocks can be adapted for clocks in a low-gravity environment. Clouds of cold atoms can be laser-prepared and then sent through a microwave

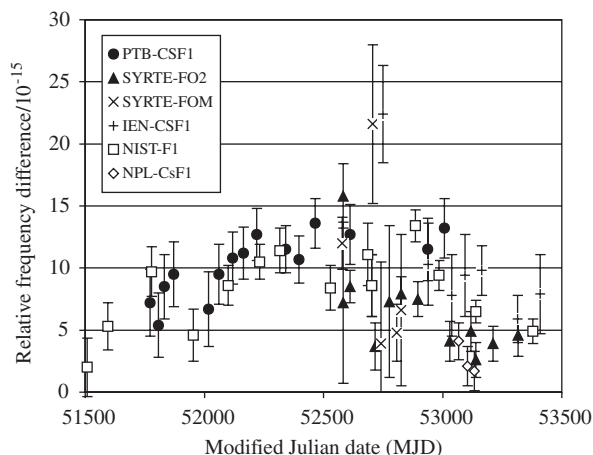


Figure 15. All contributions of atomic fountains to TAI, as of March 2005 (up to BIPM's *Circular T 206*). The 1995 to 1997 data of FO1 have been omitted for clarity.

cavity, to be detected at its end. One can expect many seconds of interaction time between atoms and microwave radiation, with resulting linewidths around 100 mHz. Three such projects for the International Space Station have been pushed ahead [105]. A NASA project, the caesium clock PARCS [106], recently became a victim of the Mars initiative of the current President of the USA. The same fate has befallen the rubidium clock experiment RACE [107], another American project. ACES [108], an ESA project, is still going ahead and is scheduled to fly to the International Space Station this decade. A major task for all space-based clocks is to develop ways of transferring the projected stability and accuracy to the ground.

The better frequency stability of a fountain clock compared with conventional beam clocks and the almost daily operation of such a fountain clock enabled the setting of a new experimental limit on the validity of the local position invariance (LPI) [109, 110], which is a part of the more general Einstein equivalence principle, which, in turn, is a foundation of Einstein's theory of general relativity. For this purpose, over the course of more than two years, the frequency difference between PTB-CSF1 and different hydrogen masers was monitored, in order to look for variations that are in phase with the time-varying gravitational potential $\Delta U(t)$ due to the annual elliptical orbital motion of the Earth. No violation of the null result predicting LPI could be detected at the level of 6×10^{-6} of the amplitude of $\Delta U(t)/c^2$ [110]. This result represents an improvement by a factor of about 100 compared with previous similar experiments and is one demonstration that significant improvements in the field of basic research become possible with the help of improved frequency standards like fountain clocks.

Atomic fountains have also been proposed for applications outside frequency metrology. For instance, the frequency of the Rabi oscillation on the clock transition is proportional to microwave power. This principle can be used to construct a microwave power standard. In the simplest case, a cloud of cold atoms can be dropped through a microwave guide [111, 112]. Alternatively, the cloud can be tossed through the microwave cavity of an atomic fountain. A proof-of-principle experiment has been performed using a small

caesium fountain, finding agreement with conventional power measurements within 5% [113].

Another proposal concerns the search for a permanent electric dipole moment (EDM) of the electron. If such an EDM existed it would mean a violation of both parity and time-reversal symmetry [114]. A typical EDM experiment searches for a change in the magnetic precession frequency of a spin-polarized sample when a strong electric field is reversed in polarity. In the proposed experiment a cloud of Yb atoms is launched in an atomic fountain [115]. Along the free-flight zone a strong homogeneous electric field can be applied. A non-zero EDM would be detected via a shift in the Ramsey pattern upon reversal of the electric field direction. A 20-fold improvement in sensitivity over the present upper limit for the electron's EDM is expected because of the long interaction time with the monokinetic sample [115].

11. Conclusion

With the advent of fountain clocks an improvement in the realization of the SI second by more than an order of magnitude over optically-pumped thermal beam clocks became a reality. The operation of fountain clocks introduced a whole new set of techniques into the routine operation of time metrology laboratories: laser cooling and manipulation of atoms. In that sense they are also paving the way for future optical clocks. In retrospect, the choice of the caesium atom as a basis for atomic time-keeping has turned out to be an extremely fortunate one because the caesium atom is one of the most readily laser-manipulated species. Just imagine: one could have chosen the hydrogen hyperfine transition instead—there would not have been an easy transition from beam clocks to laser-cooled sample clocks!

The fact that cold collision rates are almost two orders of magnitude lower in rubidium than in caesium brought up the possibility of improving the realizability of the SI second by changing its definition from the caesium to the rubidium clock transition. However, recent improvements, notably the development of the adiabatic passage method, have given the caesium definition of the SI second a new lease of life. With several caesium fountain clocks breaking the 10^{-15} barrier for relative uncertainty, some even reaching the low 10^{-16} range, the bar has been raised for potential contestants for the crown of precise time-keeping. Eventually, optical or even nuclear [116] transitions will take over, with a concomitant change of the definition of the SI second. The impressive performance of the fountain clocks of today has already eliminated some candidates for optical clocks, and will perhaps continue to do so in the years to come.

In the meantime, caesium fountain clocks serve as references for the precise determination of the frequency of optical transitions. Because it is difficult, with currently available time-transfer techniques, to remotely compare optical frequency standards situated in different laboratories, they will continue to fill this important role for some time to come. Along the way, the excellent stability of fountain clocks can help in detecting possible variations in the constants of nature, by allowing repeated comparisons of different optical and/or microwave transitions over many years [95, 117–120].

Even when, one day, the SI second will no longer be based on caesium, the fountain clocks might play the same role that thermal beam standards currently play for fountain clocks: the old, reliable workhorse for routine time-scale generation, while the new generation is being perfected.

Acknowledgments

We thank our colleagues in Paris for making available the data for figures 6 and 11–13. We thank A Bauch, C O Weiß and F Riehle for a critical reading of the manuscript.

References

- [1] Vanier J and Audoin C 2005 *Metrologia* **42** S31–42
- [2] Bauch A 2005 *Metrologia* **42** S43–54
- [3] Makdissi A and de Clercq E 2001 *Metrologia* **38** 409
- [4] Shirley J H, Lee W D and Drullinger R E 2001 *Metrologia* **38** 427
- [5] Shirley J H, Lee W D and Drullinger R E 2002 *Metrologia* **39** 123 (erratum)
- [6] Hasegawa A, Fukuda K, Kajita M, Ito H, Kumagai M, Hosokawa M, Kotake N and Morikawa T 2004 *Metrologia* **41** 257
- [7] Special issue on laser cooling 1989 *J. Opt. Soc. Am. B* **6** 2020
- [8] Forman P 1985 *Proc. IEEE* **73** 1181
- [9] De Marchi A 1982 *Metrologia* **18** 103
- [10] Hall J L, Zhu M and Buch P 1989 *J. Opt. Soc. Am. B* **6** 2194
- [11] Kasevich M A, Riis E, Chu S and DeVoe R G 1989 *Phys. Rev. Lett.* **63** 612
- [12] Clairon A, Ghezali S, Santarelli G, Laurent Ph, Lea S N, Bahoura M, Simon E, Weyers S and Szymaniec K 1996 *Proc. 5th Symp. Frequency Standards and Metrology* (Singapore: World Scientific) pp 45–59
- [13] Clairon A, Salomon C, Guellati S and Phillips W D 1991 *Europhys. Lett.* **16** 165
- [14] Jefferts S N, Meekhof D M, Shirley J H, Parker T E and Levi F 1999 *Proc. Joint Meeting 13th European Frequency and Time Forum—IEEE International Frequency Control Symp. (Besançon)* pp 12–15
- [15] Weyers S, Hübner U, Fischer B, Schröder R, Tamm Chr and Bauch A 2000 *Proc. 14th European Frequency and Time Forum (Torino)* pp 53–57
- [16] Levi F, Lorini L, Calonico D and Godone A 2004 *IEEE Trans. Ultrason. Ferroelectrics Freq. Control* **51** 1216
- [17] Szymaniec K, Chalupczak W, Whibberley P B, Lea S N and Henderson D 2005 *Metrologia* **42** 49
- [18] Vian C *et al* 2005 *IEEE Trans. Instrum. Meas.* **54** 833
- [19] Dudle G, Joyet A, Berthoud P, Mileti G and Thomann P 2001 *IEEE Trans. Instrum. Meas.* **50** 510
- [20] Domnin Yu S, Elkin G A, Novoselov A V, Kopylov L N, Baryshev V N and Pal'chikov V G 2002 *Can. J. Phys.* **80** 1321
- [21] Kumagai M, Ito H, Fukuda K, Kajita M, Hosokawa M and Morikawa T 2003 *J. Natl. Inst. Inform. Commun. Technol.* **50** 51
- [22] Kwon T Y, Lee H S, Yang S H and Park S E 2003 *IEEE Trans. Instrum. Meas.* **52** 263
- [23] Kurosu T, Fukuyama Y, Koga Y and Abe K 2004 *IEEE Trans. Instrum. Meas.* **53** 466
- [24] United States Naval Observatory 2004 *Report 2004-01 to the 16th Meeting of the CCTF*
- [25] National Institute of Metrology 2004 *Report 2004-05 to the 16th Meeting of the CCTF*
- [26] National Research Council 2004 *Report 2004-21 to the 16th Meeting of the CCTF*
- [27] Magalhaães D V, Santos M S, Bebechibuli A, Müller S T and Bagnato V S 2004 *Conf. on Precision Electromagnetic Measurements (London)*
- [28] Kumagai M, Ito H, Kajita M and Hosokawa M 2005 *Proc. 19th European Frequency and Time Forum (Besançon)*
- [29] Chu S 1998 *Rev. Mod. Phys.* **70** 685
- [30] Cohen-Tannoudji C N 1998 *Rev. Mod. Phys.* **70** 707
- [31] Phillips W D 1998 *Rev. Mod. Phys.* **70** 721
- [32] Raab E, Prentiss M, Cable A, Chu S and Pritchard D E 1987 *Phys. Rev. Lett.* **59** 2631
- [33] Chu S, Hollberg L, Bjorkholm J E, Cable A and Ashkin A 1985 *Phys. Rev. Lett.* **55** 48
- [34] Lett P D, Phillips W D, Rolston S L, Tanner C E, Watts R N and Westbrook C I 1989 *J. Opt. Soc. Am. B* **6** 2084
- [35] Simon E 1997 *Vers une stabilité et une exactitude de 10^{-16} pour les horloges atomiques: -le rayonnement du corps noir -la détection optique* *PhD Thesis* Université de Paris XI Orsay
- [36] Barrat J P and Cohen-Tannoudji C N 1961 *J. Physique Radium* **22** 329
- [37] Weyers S, Hübner U, Fischer B, Schröder R, Tamm C and Bauch A 2001 *Metrologia* **38** 343
- [38] Jefferts S R *et al* 2002 *Metrologia* **39** 321
- [39] Metcalf H J and van der Straaten P 1999 *Laser Cooling and Trapping* (New York: Springer)
- [40] Dalibard J and Cohen-Tannoudji C 1989 *J. Opt. Soc. Am. B* **6** 2023
- [41] Ungar P J, Weiss D S, Riis E and Chu S 1989 *J. Opt. Soc. Am. B* **6** 2058
- [42] Weyers S, Bauch A, Schröder R and Tamm Chr 2002 *Proc. 6th Symp. on Frequency Standards and Metrology* vol 5 (Singapore: World Scientific) p 64
- [43] Vecchi G and De Marchi A 1993 *IEEE Trans. Instrum. Meas.* **42** 434
- [44] Khurshheed A, Vecchi G and De Marchi A 1996 *IEEE Trans. Ultrason. Ferroelectrics Freq. Control* **43** 201
- [45] Jefferts S R, Drullinger R E and De Marchi A 1998 *Proc. 1998 IEEE International Frequency Control Symp. (Pasadena, CA)* vol 6, p 1082
- [46] Schröder R, Hübner U and Griebisch D 2002 *IEEE Trans. Ultrason. Ferroelectrics Freq. Control* **49** 383
- [47] Bize S *et al* 2004 *C. R. Physique* **5** 829
- [48] Barnes J A *et al* 1971 *IEEE Trans. Instrum. Meas.* **20** 105
- [49] Santarelli G, Laurent Ph, Lomonte P, Clairon A, Mann A G, Chang S, Luiten A N and Salomon C 1999 *Phys. Rev. Lett.* **82** 4619
- [50] Itano W M, Bergquist J C, Bollinger J J, Gilligan J M, Heinzen D J, Moore F L, Raizen M G and Wineland D J 1993 *Phys. Rev. A* **47** 3554
- [51] Dick G J 1987 *Proc. 19th Ann. PTTI Systems and Applications Meeting (Redondo Beach, CA)* pp 133–47
- [52] Dick G J, Prestage J D, Greenhall C A and Maleki L 1990 *Proc. 22th Ann. PTTI Systems and Applications Meeting (Vienna)* pp 497–508
- [53] Audoin C, Santarelli G, Makdissi A and Clairon A 1998 *IEEE Trans. Ultrason. Ferroelectrics Freq. Control* **45** 877
- [54] Santarelli G, Audoin C, Makdissi A, Laurent P, Dick G J and Clairon A 1998 *IEEE Trans. Ultrason. Ferroelectrics Freq. Control* **45** 887
- [55] Weyers S, Bauch A, Hübner U, Schröder R and Tamm Chr 2000 *IEEE Trans. Ultrason. Ferroelectrics Freq. Control* **47** 432
- [56] Vanier J and Audoin C 1989 *The Quantum Physics of Atomic Frequency Standards* (Bristol: Hilger)
- [57] Majorana E 1932 *Nuovo Cimento* **9** 43
- [58] Bauch A and Schröder R 1993 *Ann. Phys.* **2** 421
- [59] Itano W M, Lewis L L and Wineland D J 1982 *Phys. Rev. A* **25** 1233
- [60] Simon E, Laurent Ph and Clairon A 1998 *Phys. Rev. A* **57** 436
- [61] Bauch A and Schröder R 1997 *Phys. Rev. Lett.* **78** 622
- [62] Augustin R, Bauch A and Schröder R 1998 *Kleinheubacher Ber.* **41** 133
- [63] Augustin R, Bauch A and Schröder R 1997 *Proc. 11th European Frequency and Time Forum (Neuchâtel)* pp 47–52

- [63] Levi F, Calonico D, Lorini L, Micalizio S and Godone A 2004 *Phys. Rev. A* **70** 033412
- [64] Micalizio S, Godone A, Calonico D, Levi F and Lorini L 2004 *Phys. Rev. A* **69** 053401
- [65] Zhang S 2004 Déplacement de fréquence dû au rayonnement du corps noir dans une fontaine atomique à césium et amélioration des performances de l'horloge *PhD Thesis* Université de Paris VI
- [66] Pal'chikov V G and Domnin Yu S 2005 *19th European Frequency and Time Forum (Besançon)* (Book of Abstracts)
- [67] Feichtner J D, Hoover M E and Mizushima M 1965 *Phys. Rev.* **137** A702
- [68] Lee T, Das T P and Sternheimer R M 1975 *Phys. Rev. A* **11** 1784
- [69] Haun R D Jr and Zacharias J R 1957 *Phys. Rev.* **107** 107
- [70] Mowat J R 1972 *Phys. Rev. A* **5** 1059
- [71] Pal'chikov V G, Domnin Yu S and Novoselov A V 2003 *J. Opt. B: Quantum Semiclass Opt.* **5** S131
- [72] Tiesinga E, Verhaar B J, Stoof H T C and van Bragt D 1992 *Phys. Rev. A* **45** R2671
- [73] Leo P J, Julienne P S, Mies F H and Williams C J 2001 *Phys. Rev. Lett.* **86** 3743
- [74] Sortais Y, Bize S, Nicolas C, Clairon A, Salomon C and Williams C 2000 *Phys. Rev. Lett.* **85** 3117
- [75] Fertig C and Gibble K 2000 *Phys. Rev. Lett.* **85** 1622
- [76] Pavlis N K and Weiss M A 2003 *Metrologia* **40** 66
- [77] Luiten A, Mann A G and Blair D G 1994 *Electron. Lett.* **30** 417
- [78] Kuzmich A, Mølmer K and Polzik E 1997 *Phys. Rev. Lett.* **79** 4782
- [79] Wang R T and Dick G J 2003 *Proc. 2003 International Frequency Control Symp. and PDA Exhibition Jointly with the 17th European Frequency and Time Forum (Tampa, FL)* pp 371–5
- [80] Ertmer W, Blatt R, Hall J L and Zhu M 1985 *Phys. Rev. Lett.* **54** 996
- [81] Marion H 2005 Contrôle des collisions froides du ^{133}Cs , test de la variation de la constante de structure fine à l'aide d'une fontaine atomique double rubidium-césium *PhD Thesis* Université de Paris VI
- [82] Joyet A, Mileti G, Dudle G and Thomann P 2001 *IEEE Trans. Instrum. Meas.* **50** 150
- [83] Joyet A 2003 Aspects métrologiques d'une fontaine continue à atoms froids *PhD Thesis* Université de Neuchâtel
- [84] Di Domenico G, Castagna N, Mileti G, Thomann P, Taichenachev A V and Yudin V I 2004 *Phys. Rev. A* **69** 063403
- [85] Taichenachev A V, Tumaikin A M, Yudin V I and Hollberg L 2001 *Phys. Rev. A* **63** 033402
- [86] Castagna N, Di Domenico G, Dudle G, Plimmer M D, Taichenachev A V, Thomann P and Yudin V I 2005 *19th European Frequency and Time Forum (Besançon)* (Book of Abstracts) p 55
- [87] Fertig C and Gibble K 1998 *Phys. Rev. Lett.* **81** 5780
- [88] Fertig C, Rees J I and Gibble K 2001 *Proc. 2001 International Frequency Control Symp. and PDA Exhibition (Seattle, WA)* pp 18–21
- [89] Levi F, Godone A and Lorini L 2001 *IEEE Trans. Ultrason. Ferroelectrics Freq. Control* **48** 847
- [90] Jefferts S R, Heavner T P, Donley E A, Shirley J H and Parker T E 2003 *Proc. 2003 IEEE International Frequency Control Symp. and PDA Exhibition Jointly with the 17th European Frequency and Time Forum (Tampa, FL)* pp 1084–8
- [91] Heavner T P, Jefferts S R, Donley E A, Shirley J H and Parker T E 2005 submitted for publication
- [92] Pereira Dos Santos F, Marion H, Bize S, Sortais Y and Clairon A 2002 *Phys. Rev. Lett.* **89** 233004
- [93] Camparo J C and Frueholz R P 1984 *J. Phys. B: At. Mol. Phys.* **17** 4169
- [94] Marion H *et al* 2004 *Proc. 18th European Frequency and Time Forum (Guildford)* p 10
- [95] Marion H *et al* 2003 *Phys. Rev. Lett.* **90** 150801
- [96] Kokkelmans S J J M F, Verhaar B J, Gibble K and Heinzen D J 1997 *Phys. Rev. A* **56** R4389
- [97] Sortais Y, Bize S, Nicolas C, Santarelli G, Salomon C and Clairon A 2000 *IEEE Trans. Ultrason. Ferroelectrics Freq. Control* **47** 1093
- [98] Bize S, Sortais Y, Santos M S, Mandache C, Clairon A and Salomon C 1999 *Europhys. Lett.* **45** 558
- [99] CCTF 2004 *Recommendation CCTF-1 2004 concerning secondary representations of the second* p 38
- [100] Heavner T P, Jefferts S R, Donley E A, Shirley J H and Parker T E 2005 *IEEE Trans. Instrum. Meas.* **54** 842
- [101] Li R and Gibble K 2004 *Metrologia* **41** 376
- [102] Bauch A 2003 *Meas. Sci. Technol.* **14** 1159
- [103] Richard J-Y *et al* 2004 *Proc. 18th European Frequency and Time Forum (Guildford)* p 64
- [104] Bize S, Marion H, Clairon A, Calonico D, Lorini L, Levi F, Szymaniec K, Chalupczak W and Henderson D 2005 *Proc. 19th European Frequency and Time Forum (Besançon)*
- [105] Lämmerzahl C *et al* 2004 *Gen. Rel. Grav.* **36** 615
- [106] Jefferts S R *et al* 1999 *Proc. Joint Meeting of the European Frequency and Time Forum—IEEE International Frequency Control Symp. (Besançon)* pp 141–4
- [107] Fertig C, Gibble K, Klipstein B, Maleki L, Seidel D and Thompson R 2000 *Proc. 2000 International Frequency Control Symp. (Kansas City, MO)* p 676
- [108] Salomon C *et al* 2001 *C. R. Acad. Sci.* **2** 1313
- [109] Bauch A and Weyers S 2002 *Phys. Rev. D* **65** R081101
- [110] Bauch A, Nelson L, Parker T and Weyers S 2003 *Proc. 2003 International Frequency Control Symp. and 17th European Frequency and Time Forum (Tampa, FL)* pp 217–21
- [111] Paulusse D C, Rowell N L and Michaud A 2002 *Digest of the Conference on Precision Electromagnetic Measurements CPEM 2002 (Ottawa, Canada)* pp 194–5
- [112] Paulusse D C, Rowell N L and Michaud A 2005 *IEEE Trans. Instrum. Meas.* **54** 692
- [113] Donley E A, Crowley T P, Heavner T P and Riddle B F 2003 *Proc. 2003 International Frequency Control Symp. and 17th European Frequency and Time Forum (Tampa, FL)* pp 135–7
- [114] Khriplovich I B 1991 *Parity Nonconservation in Atomic Phenomena* (Philadelphia: Gordon and Breach)
- [115] Natarajan V 2005 *Eur. Phys. J. D* **32** 33
- [116] Peik E and Tamm Chr 2003 *Europhys. Lett.* **61** 181
- [117] Bize S *et al* 2003 *Phys. Rev. Lett.* **90** 150802
- [118] Karshenboim S and Peik E (ed) 2004 *Astrophysics, Clocks and Fundamental Constants* (Berlin: Springer)
- [119] Fischer M *et al* 2004 *Phys. Rev. Lett.* **92** 230802
- [120] Peik E, Lipphardt B, Schnatz H, Schneider T, Tamm Chr and Karshenboim S G 2004 *Phys. Rev. Lett.* **93** 170801